2014 International Conference on Unmanned Aircraft Systems (ICUAS)
May 27-30, 2014. Orlando, FL, USA

Obstacle Detection and Navigation Planning for Autonomous Micro Aerial Vehicles

Matthias Nieuwenhuisen, David Droeschel, Marius Beul, and Sven Behnke

***Abstract*— Obstacle detection and real-time planning of collision-free trajectories are key for the fully autonomous operation of micro aerial vehicles in restricted environments.**

In this paper, we propose a complete system with a multimodal sensor setup for omnidirectional obstacle perception consisting of a 3D laser scanner, two stereo camera pairs, and ultrasonic distance sensors. Detected obstacles are aggregated in egocentric local multiresolution grid maps. We generate trajectories in a multi-layered approach: from mission planning to global and local trajectory planning, to reactive obstacle avoidance.

We evaluate our approach in simulation and with the real autonomous micro aerial vehicle.

I. Introduction

Micro aerial vehicles (MAVs) are enjoying increasing popularity. Due to their low cost and flexibility, they are used for aerial photography, inspection and surveillance missions. In most cases, a human operator pilots the MAV remotely to fulfill a specific task or the MAV is following a predefined path of GPS waypoints in an obstacle-free altitude.

Our MAV is shown in Fig. 1. We aim for a fully autonomous creation of semantic maps of buildings on demand of a user. Hence, the MAV has to operate at low altitudes in the vicinity of facades and other structures, e.g., trees, street lights, and power cables. This requires more elaborated means of navigation than direct flight between predefined GPS waypoints. We follow a multi-layered approach to navigation: from slower deliberative to fast reactive layers, including mission planning, global and local path planning, fast local obstacle avoidance, and robust motion controllers.

Although we aim at mapping the environment during execution, prior knowledge can aid our mission planning—in contrast to fully autonomous exploration of unknown space. We incorporate 3D city models as acquired by land surveying authorities, i.e., a Level-of-Detail 2 (LoD2) model containing footprint, height, and roof-shape of buildings [1] and a digital elevation model (DEM) of the environment. These models do not include smaller structures, which constitute a collision hazard for the MAV. Thus, the initial mission plans need to be adjusted on the fly, whenever more information becomes available during a flight. Nevertheless, buildings are often the largest obstacles and might inhibit local path planners to find a feasible path towards the global goal. Other obstacles, e.g., power poles, vegetation, or building attachments, are likely to be small enough to be covered by our local obstacle map, built by means of efficient multiresolution scan registration. Hence, a globally consistent path enables a local planner to navigate towards a global goal.

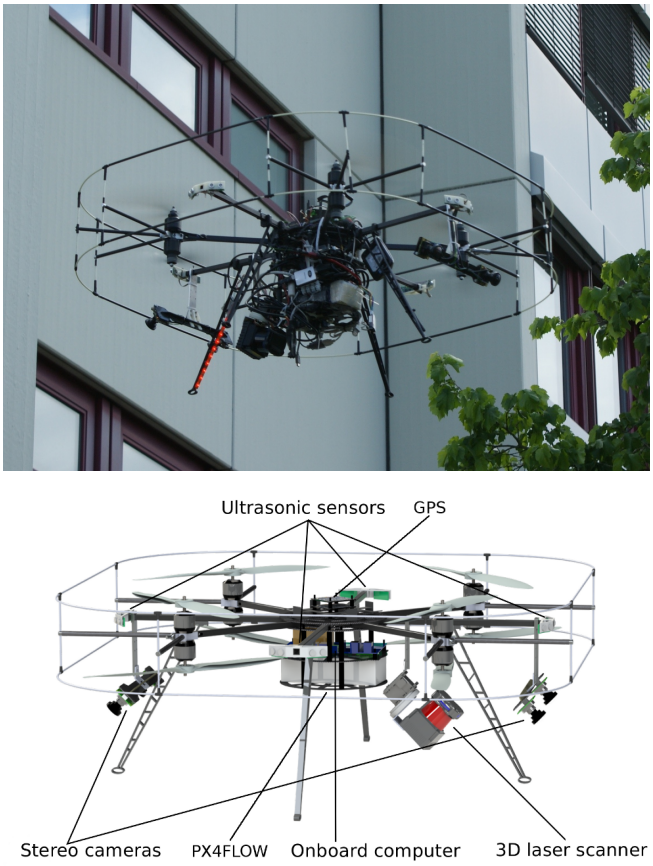

Fig. 1: Our MAV is equipped with eight co-axial rotors and a plurality of sensors, including a continuously rotating 3D laser scanner and two stereo camera pairs.

MAVs pose a problem for designing sensory systems and perception algorithms due to their size and weight constraints and limited computing power. In order to enable navigation in difficult 3D environments for autonomous MAVs, we developed a small and lightweight continuously rotating 3D laser scanner that measures distances of up to 30 m in almost all directions. It consists of a Hokuyo 2D laser range finder (LRF) which is rotated by a servo actuator to gain a 3D FoV, as shown in Fig. 2.

Up to now, such 3D laser scanners are rarely used on MAVs due to their payload limitations. Instead, two-

This work has been supported by grants BE 2556/7 and BE 2556/8 of German Research Foundation (DFG).

The authors are with the Autonomous Intelligent Systems Group, Institute for Computer Science VI, University of Bonn, Germany nieuwenh@ais.uni-bonn.de

dimensional laser range finders are used [2], [3], [4], [5], which restricts the field-of-view to the two-dimensional measurement plane.

Additionally, our MAV is equipped with two stereo camera pairs, and ultrasonic sensors covering the volume around the MAV up to 30 m range [6]. All these sensors have only local precision. This is reflected in the local multiresolution property of our MAV-centric obstacle map. The local navigation planner operates directly on this representation. We employ 3D local multiresolution path planning, extending ideas from our prior work [7]. This efficient planning technique allows for frequent replanning, which makes 3D navigation in dynamic, unpredictable environments possible.

After a discussion of related work in the next section, we introduce our MAV in Sec. III. Sec. IV describes our local multiresolution obstacle map. Our hierarchical control architecture from global path planning to low-level control is detailed in Sec. V. We present evaluation results in Sec. VI.

II. Related Work

The application of MAVs varies especially in the level of autonomy—ranging from basic hovering and position holding [8] over trajectory tracking and waypoint navigation [9] to fully autonomous navigation [2].

1) Obstacle Perception: Particularly important for fully autonomous operation is the ability to perceive obstacles and to avoid collisions. Obstacle avoidance is often neglected, e.g., by flying in a sufficient height when autonomously flying between waypoints. Most approaches to obstacle avoidance for MAVs are camera-based, due to the limited payload [10], [11], [12], [13], [14], [15], [16], [17]. Hence, collision avoidance is restricted to the field of view (FoV) of the cameras. Moore et al. [18] use a ring of small cameras to achieve an omnidirectional view in the horizontal plane, but rely on optical flow for speed control, centering, and heading stabilization only.

Other groups use 2D laser range finders (LRF) to localize the UAV and to avoid obstacles [2], limiting obstacle avoidance to the measurement plane of the LRF, or combine LRFs and visual obstacle detection [3], [19], [20]. Still, their perceptual field is limited to the apex angle of the stereo camera pair (facing forwards), and the 2D measurement plane of the scanner when flying sideways. They do not perceive obstacles outside of this region or behind the vehicle.

We allow omnidirectional 4D movements of our MAV, thus we have to take obstacles in all directions into account. Another MAV with a sensor setup that allows omnidirectional obstacle perception is described in [21].

2) Navigation Planning: A two-level approach to collision-free navigation using artificial potential fields on the lower layer is proposed in [22]. Similar to our work, completeness of the path planner is guaranteed by an allocentric layer on top of local collision avoidance.

Some reactive collision avoidance methods for MAVs are based on optical flow [23] or a combination of flow and stereo vision [24]. However, solely optical flow-based solutions cannot cope well with frontal obstacles and these methods are not well suited for omnidirectional obstacle avoidance as needed for our scenario.

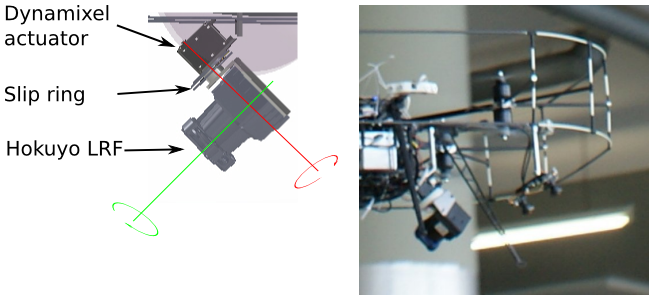

Fig. 2: 3D laser scanner. A 2D LRF is continuously rotated around the red axis.

Recent search-based methods for obstacle-free navigation include work of MacAllister et al. [25] and Cover et al. [26]. A good survey on approaches to motion planning for MAVs is given in [27]. These methods assume complete knowledge of the scene geometry—an assumption that we do not make here.

III. System Setup

Our MAV platform is an octorotor platform with a co-axial arrangement of rotors (see Fig. 1). This yields a compact flying platform that is able to carry a plurality of sensors and an onboard computer with sufficient computing power (Intel Core i7-3820QM 2.7 GHz) for sensor data processing and navigation planning employing the Robot Operating System (ROS [28]) as middleware. For low-level velocity and attitude control the MAV is equipped with a PIXHAWK flight control unit [29]. To allow for safe omnidirectional operation of the MAV in challenging environments our MAV is equipped with a multimodal sensor setup. Our main sensor for obstacle perception is a continuously rotating 3D laser scanner (Fig. 2). The measurement density of the 3D laser scanner varies and has its maximum in a forward-facing cone. Only a small portion above the MAV's back is occluded by its core. Two stereo camera pairs (pointing in forward and backward direction) are used for visual odometry and obstacle perception. Equipped with fish-eye lenses they cover a large area around the MAV. Eight ultrasonic sensors around the MAV complete the perception setup. Despite their limited range and accuracy, they aid the perception of small obstacles in the vicinity of the MAV, such as tree branches, overhead power cables and transmission lines. The fusion of these sensors facilitate the reliable detection and avoidance of obstacles. Their fusion is discussed in Sec. IV-C.

For localization and state estimation, we use GPS and an optical flow camera [30] in addition to the two stereo camera pairs and the 3D laser scanner. The flow camera is pointing vertically to the ground and can—given suitable lighting conditions—measure velocities relative to the ground-plane with more than 100 Hz. We detail our sensor setup and the processing pipeline in [6], [31].

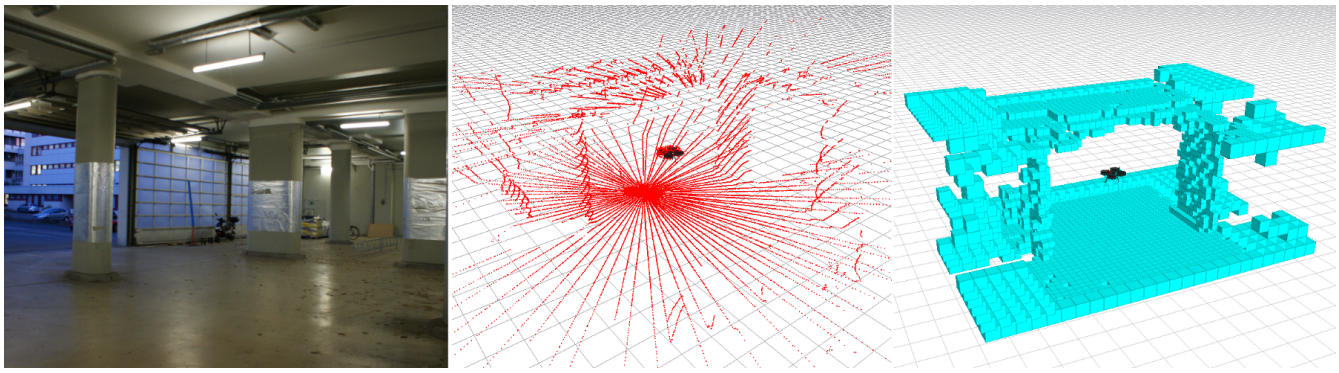

Fig. 3: We aggregate 3D laser scans (middle) into local grid-based obstacle maps. The right image shows a resulting map from the indoor environment in the left image. The scans are aggregated over 1 s.

IV. Obstacle Perception

In order to fuse and accumulate laser range measurements, we construct MAV-centric obstacle maps. For each measurement and the corresponding 3D point, the individual cell of the map is marked as occupied. An exemplary map from an indoor environment is shown in Fig. 3. The map is used by our path planning and obstacle avoidance algorithms described in subsequent sections.

A. Local Multiresolution Map

We use a hybrid local multiresolution map that represents both occupancy information and the individual distance measurements. The most recent measurements are stored in ring buffers within grid cells that increase in size with distance from the robot's center. Thus, we gain a high resolution in the close proximity to the sensor and a lower resolution far away from our robot, which correlates with the sensor's characteristics in relative distance accuracy and measurement density. Compared to uniform grid-based maps, multiresolution leads to the use of fewer grid cells without loosing information and consequently results in lower computational costs. Fig. 4 shows our multiresolution grid-based map.

We aim for efficient map management for translation and rotation. Therefore, individual grid cells are stored in a ring buffer to allow shifting of elements in constant time.

We interlace multiple ring buffers to obtain a map with three dimensions. The length of the ring buffers depends on the resolution and the size of the map. In case of a translation of the MAV, the ring buffers are shifted whenever necessary to maintain the egocentric property of the map.

B. Scan Registration

To compensate the sensor's motion during scan acquisition, we incorporate a visual odometry estimate from two pairs of wide-angle stereo cameras [32]. This 6D motion estimate is used to assemble the individual 2D scan lines of each a half rotation to a 3D scan.

We register consecutive 3D scans by matching Gaussian point statistics in grid cells (surfels) between local multiresolution grid maps [33]. We assign surfels in a probabilistic way within a Gaussian mixture model (GMM) in a coarse-to-fine fashion, which is facilitated by the multiresolution property of our map.

After the new scan has been registered to the map, the new measurements are added, replacing the oldest measurements. We also implement an aging of the individual grid cells, which leads to the abandoning of outdated measurements in free or unobserved volumes.

C. Occupancy Mapping

The individual sensors of our MAV have different strengths and weaknesses. In order to perceive as many obstacles as possible it is necessary to fuse the measurements adequately into a single map. We collect these measurements in an occupancy grid maintaining occupancy probabilities. We fuse measurements from the 3D laser scanner, from wide-angle stereo cameras and from ultrasound sensors. Fig. 5 shows an example of an outdoor scenario where fusing laser range measurements with dense stereo [34] allows for perception of challenging obstacles. Besides very thin obstacles such as a cable in the previous example, transparent objects are demanding for reliable obstacle perception. Fig. 6 shows how fusing measurements from our 3D laser scanner with ultrasound measurements allows for detecting transparent obstacles, like windows.

V. Planning

To reduce the planning complexity we divide the overall planning problem into multiple problems with different levels of abstractions. This is represented by a hierarchical control architecture for our MAV, with slower deliberative planners that solve complex path and mission planning problems on the upper layers and high-frequency reactive controllers on the lower layers (see Fig. 7).

A. Mission and Global Path Planning

The topmost layers are a mission planner and a global path planner using a static representation of the environment derived from a 3D city model and a digital elevation model, depicted in Fig. 8(a). This model is stored efficiently in an OctoMap [35]. The global environment model does not change during a single observation mission. Hence, the

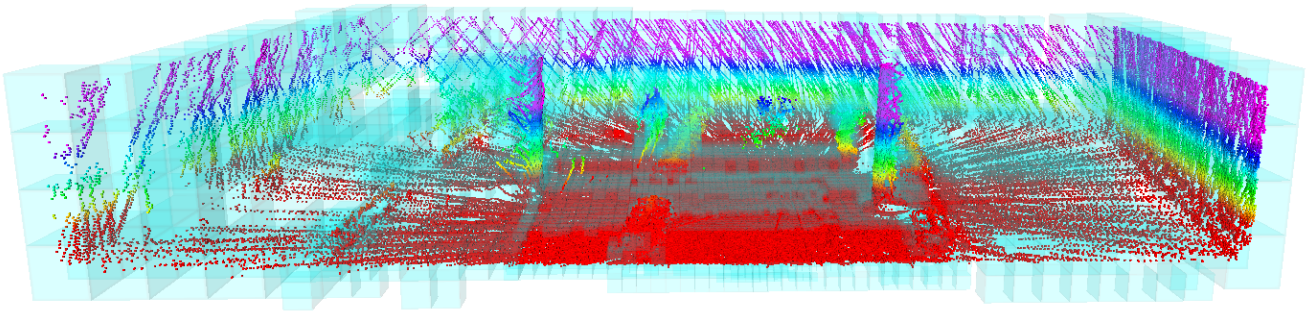

Fig. 4: Grid-based local multiresolution map with a higher resolution in proximity to the sensor and a lower resolution with increasing distance. Color encodes height.

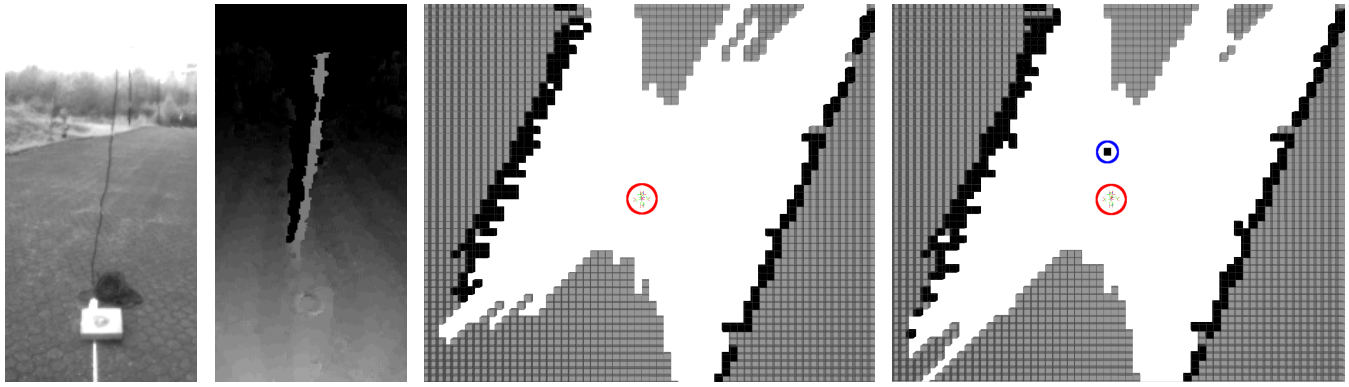

(a) (b) (c) (d)

Fig. 5: Obstacle perception by fusing laser range measurements of our 3D laser scanner with dense stereo measurements. (a) a loose-hanging cable at 3 m distance, which is not perceived with the 3D laser scanner of the MAV; (b) dense stereo allows for detecting the cable; (c) the resulting occupancy grid map with measurements from the laser scanner solely; (d) the resulting occupancy grid map with laser and dense stereo. The fused map shows the obstacle circled in blue. The position of the MAV is circled red.

(a) (b) (c) (d)

Fig. 6: Obstacle perception by fusing laser range measurements of our 3D laser scanner with ultrasound measurements. (a) a windows in 2 m distance. (b) the window is only partially perceived by the 3D laser scanner; (c) the resulting occupancy grid map with measurements from the laser scanner solely; (d) the resulting occupancy grid map with laser and ultrasound measurements (red cones). The position of the MAV is circled red.

mission planner is executed once at the beginning of a mission, necessary local deviations from the planned mission are handled on lower layers. The input to the mission planner are view poses defined by an user. It employs a global path planner on a coarse uniform grid map to determine the approximate costs between every pair of mission goals. The optimal path covering all mission objectives is solved by means of Concorde [36], a fast solver for the traveling

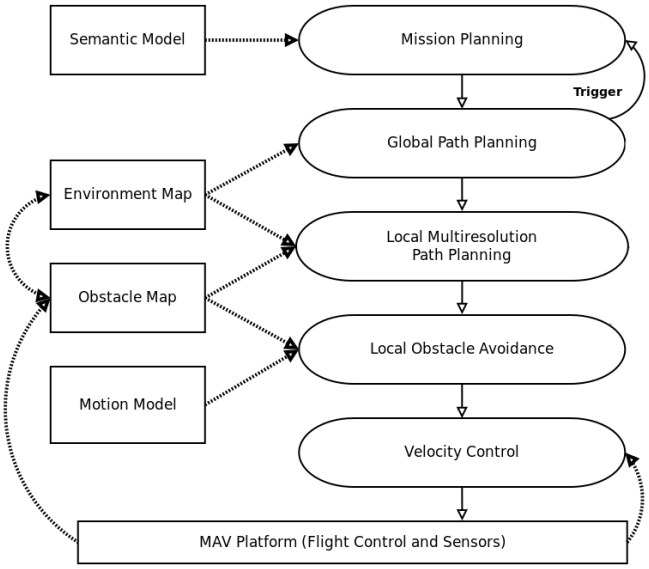

Fig. 7: Our MAV navigation concept. Slow planners on the top yield coarse trajectories which are refined on faster lower layers.

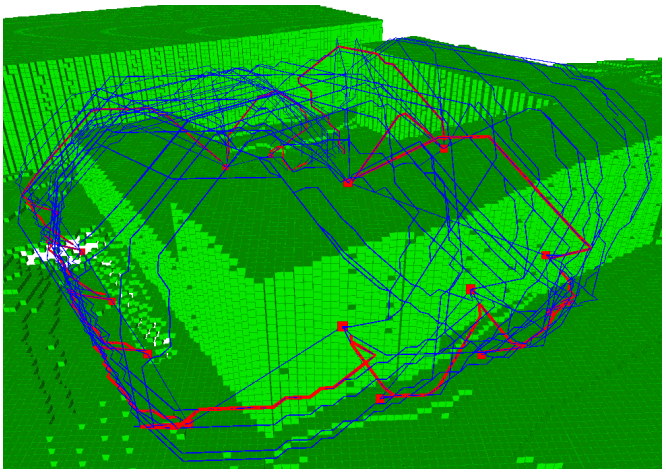

Fig. 9: On the top layer, a mission planner evaluates the best execution order of mission poses (red rectangles). Blue lines show all cost-optimal trajectories between each pair from the set of mission waypoints. The optimal flight plan to reach all waypoints is shown in red. The cost function allows for positions close to the building but penalizes these more than paths farther away.

salesman problem (TSP). Please note, that the instances of the TSP for one mission are sufficiently small and exact solutions are tractable. The result of mission planning is a flight plan composed of a list of waypoints the MAV should pass approximately or reach exactly, depending on the mission objectives. Fig. 9 shows an example solution for inspecting a part of the building complex depicted in Fig. 8.

On the next level of the control hierarchy, global planning finds a cost-optimal 3D path from the current MAV position to the next waypoint. Even though global replanning seems to be necessary only if unforeseen obstacles block mission goals and local planning is not sufficient to find a feasible detour, we found that continuous replanning is advantageous on MAVs. Our global planner runs at $0.1\,\mathrm{Hz}$ to both cope with newly acquired obstacles and react on deviations from the planned path by, e.g., gusts of wind. The global map can be updated with local sensor measurements for that case. The planned global path is fed as input to the next layer, the local path planner.

B. Local Multiresolution Planning

On the local path planning layer, we employ a 3D local multiresolution path planner. This layer plans based on the next waypoint on the global path, a local excerpt of the global map, and local distance measurements which have been aggregated in a 3D local multiresolution map (Sec. IV-A). It refines the global path according to the actual situation and a finer trajectory is fed to the potential field-based reactive obstacle avoidance layer on the next level (cf. Sec. V-C).

To resemble the relative accuracy of onboard sensors—i.e., they measure the vicinity of the robot more accurate and with higher density than distant space—we plan with a higher resolution close to the robot and with coarser resolutions with increasing distance.

Furthermore, the necessity for modifications to the plan is more probable in the future. Thus, it is reasonable to spend more effort into a finer plan in the near future. Overall, our approach reduces the planning time and makes frequent replanning feasible. Our representation consists of multiple robot-centered 3D grids. Recursively, these grids are embedded into the next coarser grid with cells with a doubled edge length. In contrast to a uniform grid that needs $\mathcal{O}(n^3)$ cells to cover a volume, our multiresolution grid needs only $\mathcal{O}(\log(n)^3)$ cells. The advantages of this representation are the low memory requirements and the inherent representation of uncertainties in sensing and motion of the MAV.

For planning within this grid, we embed an undirected graph and employ the A* algorithm. Grid cells are connected to all surrounding neighbors. Fig. 10 illustrates the result of local navigation planning for an example.

C. Local Obstacle Avoidance

On the next lower layer, we employ a fast reactive collision avoidance module based on artificial potential fields [37] as a safety measure reacting directly on the available sensor inputs.

The robot-centered local multiresolution occupancy grid, the current motion state x_t, and a target waypoint w_t, serve as input to our algorithm. The obstacle map induced repulsive forces on the MAV with magnitude $F_r^p = \mathrm{costs}\left(argmin_o\left(\|o-p\|\right)\right)$ for an obstacle o at a position p. The target waypoint induces an attractive force towards the goal.

In contrast to the standard potential field-based approach, we relax the assumption that the robot is an idealized particle. We account for the shape of the MAV by discretizing it into cells of the minimum cell size of our 3D grid map (blue grid

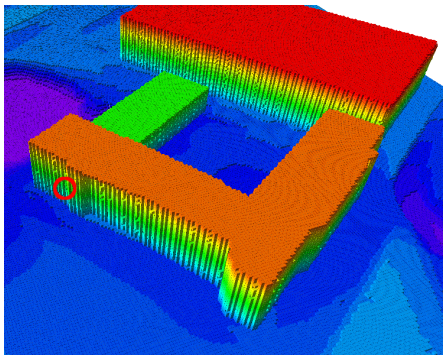

(a) OctoMap derived from the 3D city model and a digital elevation model.

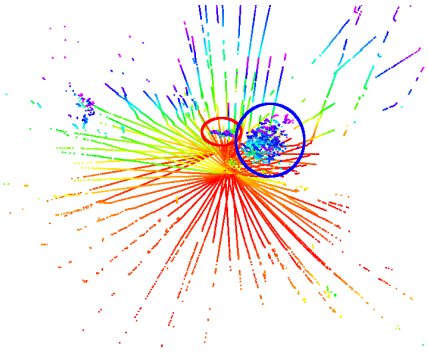

(b) Local laser scan from the environment, including a building and vegetation (blue circle). Measurements on the MAV itself are circled red.

(c) Photo of the scanned environment.

Fig. 8: For the more abstract high-level planning layers we employ coarse models of the environment, i.e., a 3D city model and a digital elevation model as provided by land surveying authorities (left). The planned paths are refined during a mission by means of the local planning and obstacle avoidance layers operating with onboard sensor measurements, e.g., 3D laser scans (middle). The color in both figures depicts the height. The MAV's position is circled red in all figures.

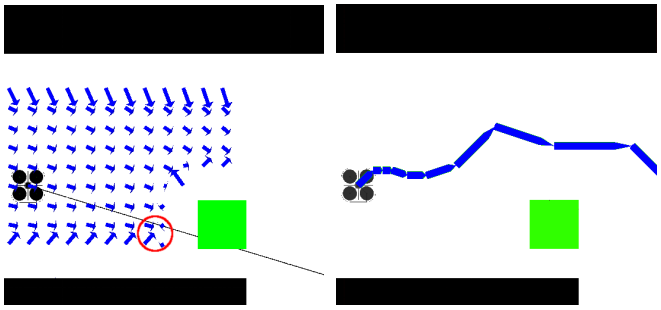

Fig. 10: Our reactive collision avoidance layer is a fast mean to react on apriori unknown obstacles (green rectangle in this example). The arrows in the left figure depict the artificial potential forces pushing the MAV away from all static and dynamic obstacles, but the MAV will get stuck in a local minimum (red circle) while approaching a waypoint in the direction of the black line. The local path planning layer is necessary to proceed without planning a new global path (right).

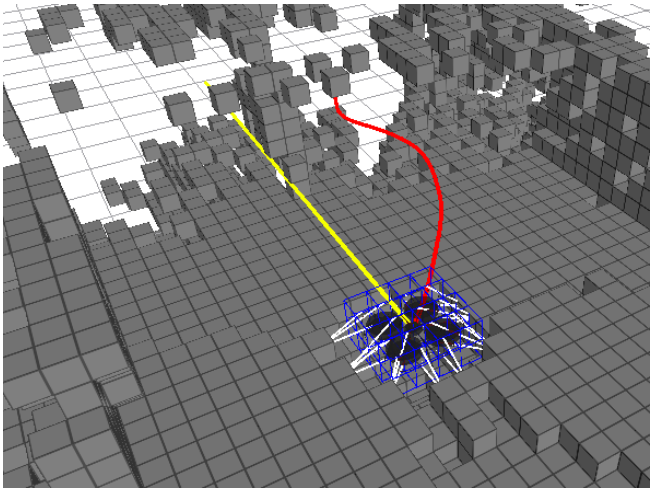

Fig. 11: We predict the influence of a motion command by rolling out the robot's trajectory (red) using a learned motion model. The direct line towards the next specified waypoint is depicted in yellow. The white lines connect obstacles to the parts of the robot model their artificial force is applied to.

cells in Fig. 11). Every cell is considered as one particle to the algorithm.

To take the MAV's dynamic state into account, we predict its future trajectory T_t by predicting the probable sequence of motion commands $u_{t:t+n}$ for a fixed discrete-time horizon n (Fig. 11). The property that multicopters can quickly change their motion state,e.g., by stopping completely and accelerating into a different direction, bounds the relevant prediction horizon.

The prediction of the future trajectory for the next n time steps, initial motion command u_0, initial position p_0, and a motion model $f(x,u)$ is then given by

$$T_t = p_{t:t+n} = (p_t, p_t+1, \ldots, p_{t+n}), \quad (1)$$

$$p_{i+1} = f(x_i, u_i) + p_i \qquad i \in [t : t+n-1], \quad (2)$$

$$u_i = C\vec{F}_{p_i}. \quad (3)$$

The future control commands u_i are predicted by mapping the estimated forces $\vec{F}_{p_i}$ at a position p_i to a control command with matrix C. If a given force threshold is exceeded at any point p_i of the trajectory, we reduce the velocity v of the MAV to

$$v_{new} = \left(\frac{1}{2} + \frac{i}{2n}\right) v_{max}. \quad (4)$$

For more details, see [38].

VI. Evaluation

A. Global Path Planning

We tested our global path planner in simulation and with the real MAV. In the real robot experiments our MAV had

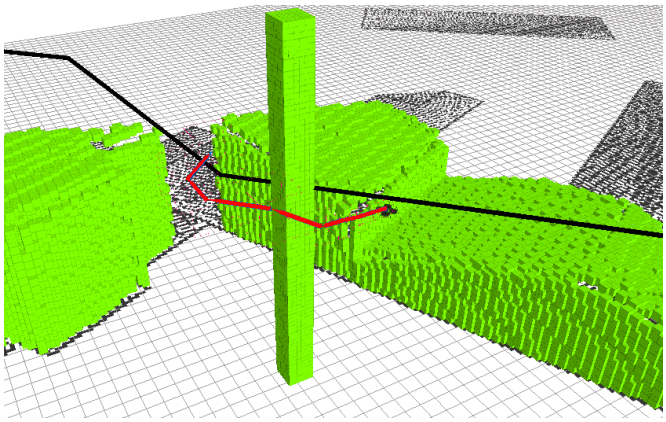

Fig. 13: Globally consistent paths (black lines) are planned based on a static environment model at 0.1 Hz. A local multiresolution path planner incorporating sensor information refines the path locally (red lines) to avoid newly perceived obstacles, e.g., the pole in this example situation.

TABLE I: Planning time (in milliseconds) and normalized lengths of resulting trajectories.

grid representation	cell size (in m)	planning time min.	planning time max.	length
multiresolution	0.25	12	35	1.03
uniform	0.25	26	3395	1.00
uniform	1.00	4	20	1.09

to follow the planned paths employing a position controller and GPS. We extended the allocentric map derived from city and elevation model with obstacles (lanterns) for these experiments. Replanning was performed at 0.1 Hz and all components were running on the onboard computer. Our MAV was able to follow the planned paths collision free. Fig. 12 shows an example from the test runs where the MAV was pushed from the planned path by a gust of wind resulting in a qualitatively different path after replanning.

B. Local Path Planning

We evaluate the computing time and the resulting flight trajectories in simulation. The MAV follows a globally planned path and has to avoid obstacles that are not in the apriori known world model (Fig. 13). The experiments were performed with two different uniform grids with cell size 0.25 m and 1 m, respectively. These were compared to our local multiresolution grid with a minimum cell size of 0.25 m and 8 cells per grid. The timings in Tab. I are measured with the MAV's onboard computer.

All planning representations perform equally well if the globally planned path can be followed. In the case newly perceived obstacles have to be surrounded, the planning time increases using a uniform grid with high resolution substantially exceeds the time window for replanning. In contrast, the local multiresolution planning is always fast enough for continuous replanning.

Tab. I summarizes the resulting path lengths for a case where the MAV has to locally plan a detour around an obstacle not represented in the static environment model using the three planning representations. The path lengths are normalized for comparability between test runs. Local obstacle avoidance without global replanning results in 3% longer paths by means of our proposed multiresolution grid instead of the fine uniform grid. The coarse uniform grid results in 9% longer paths.

VII. Conclusions

In this paper, we presented an integrated system to operate MAVs safely in the vicinity of obstacles. In the vicinity of structures, fast reactions on new obstacle perceptions are inevitable. We approach this challenge by employing local multiresolution mapping and planning techniques that facilitate frequent updates and replanning. This refines higher-level mission plans based on onboard sensing. A reactive collision avoidance layer accounts for fast MAV and environment dynamics.

References

[1] G. Gröger, T. H. Kolbe, A. Czerwinski, and C. Nagel, "Opengis city geography markup language (citygml) encoding standard," *Open Geospatial Consortium Inc. Reference number of this OGC® project document: OGC*, 2008.

[2] S. Grzonka, G. Grisetti, and W. Burgard, "A fully autonomous indoor quadrotor," *IEEE Trans. on Robotics*, vol. 28, no. 1, pp. 90–100, 2012.

[3] T. Tomić, K. Schmid, P. Lutz, A. Domel, M. Kassecker, E. Mair, I. Grixa, F. Ruess, M. Suppa, and D. Burschka, "Toward a fully autonomous UAV: Research platform for indoor and outdoor urban search and rescue," *Robotics Automation Magazine, IEEE*, vol. 19, no. 3, pp. 46–56, 2012.

[4] A. Bachrach, R. He, and N. Roy, "Autonomous flight in unstructured and unknown indoor environments," in *Proc. of European Micro Aerial Vehicle Conf. (EMAV)*, 2009.

[5] S. Shen, N. Michael, and V. Kumar, "Autonomous multi-floor indoor navigation with a computationally constrained micro aerial vehicle," in *Proc. of IEEE Int. Conf. on Robotics and Automation (ICRA)*, 2011.

[6] D. Holz, M. Nieuwenhuisen, D. Droeschel, M. Schreiber, and S. Behnke, "Towards mulimodal omnidirectional obstacle detection for autonomous unmanned aerial vehicles," in *Int. Arch. Photogramm. Remote Sens. Spatial Inf. Sci. (ISPRS)*, vol. XL-1/W2, 2013, pp. 201–206.

[7] S. Behnke, "Local multiresolution path planning," *Robocup 2003: Robot Soccer World Cup VII*, pp. 332–343, 2004.

[8] S. Bouabdallah, P. Murrieri, and R. Siegwart, "Design and control of an indoor micro quadrotor," in *Proc. of IEEE Int. Conf. on Robotics and Automation (ICRA)*, 2004.

[9] T. Puls, M. Kemper, R. Kuke, and A. Hein, "GPS-based position control and waypoint navigation system for quadrocopters," in *Proc. of IEEE/RSJ Int. Conf. on Intelligent Robots and Systems (IROS)*, 2009.

[10] T. Mori and S. Scherer, "First results in detecting and avoiding frontal obstacles from a monocular camera for micro unmanned aerial vehicles," in *Proc. of IEEE Int. Conf. on Robotics and Automation (ICRA)*, 2013.

[11] S. Ross, N. Melik-Barkhudarov, K. S. Shankar, A. Wendel, D. Dey, J. A. Bagnell, and M. Hebert, "Learning monocular reactive uav control in cluttered natural environments," in *Proc. of IEEE Int. Conf. on Robotics and Automation (ICRA)*, 2013.

[12] K. Schmid, P. Lutz, T. Tomić, E. Mair, and H. Hirschmüller, "Autonomous vision-based micro air vehicle for indoor and outdoor navigation," *Journal of Field Robotics*, 2014.

[13] D. Magree, J. G. Mooney, and E. N. Johnson, "Monocular visual mapping for obstacle avoidance on UAVs," *Journal of Intelligent & Robotic Systems*, vol. 74, no. 1-2, pp. 17–26, 2014.

[14] A. Tripathi, R. G Raja, and R. Padhi, "Reactive collision avoidance of UAVs with stereovision camera sensors using UKF," in *Advances in Control and Optimization of Dynamical Systems*, vol. 3, no. 1, 2014, pp. 1119–1125.

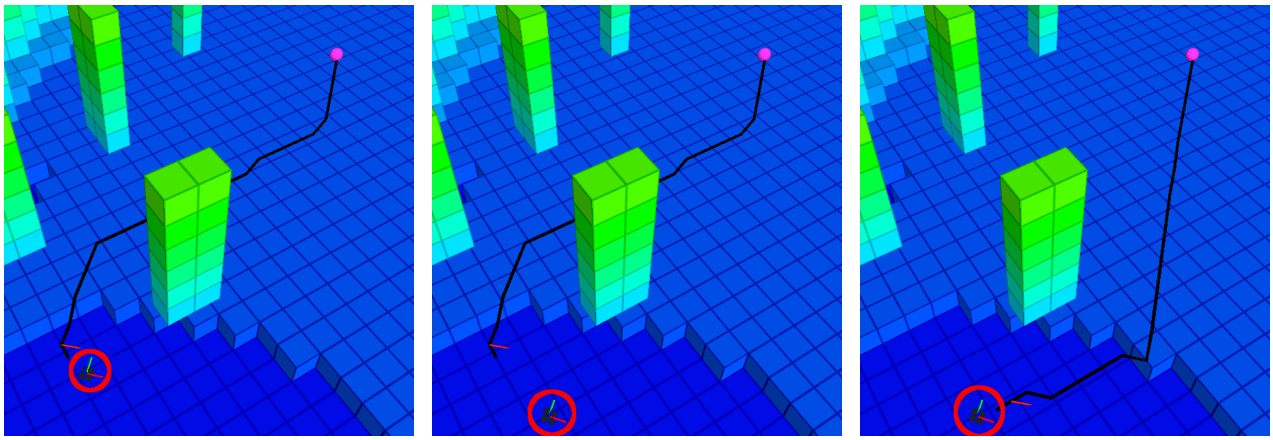

Fig. 12: While following an allocentric planned path (black lines) given a static environment map (left) our MAV was disturbed by a strong gust of wind (middle). By continuous replanning a new cost-optimal path to the goal waypoint could be found (right) and the MAV reached the goal collision free. The red circle highlights the position of the MAV, the pink dot the goal, and the red arrow the next intermediate waypoint to reach.

[15] G. Flores, S. Zhou, R. Lozano, and P. Castillo, "A vision and GPS-based real-time trajectory planning for a MAV in unknown and low-sunlight environments," *Journal of Intelligent & Robotic Systems*, vol. 74, no. 1-2, pp. 59–67, 2014.

[16] K. Schauwecker and A. Zell, "On-board dual-stereo-vision for the navigation of an autonomous MAV," *Journal of Intelligent & Robotic Systems*, vol. 74, no. 1-2, pp. 1–16, 2014.

[17] J. Park and Y. Kim, "3d shape mapping of obstacle using stereo vision sensor on quadrotor uav," in *AIAA Guidance, Navigation, and Control Conference*, 2014.

[18] R. Moore, K. Dantu, G. Barrows, and R. Nagpal, "Autonomous MAV guidance with a lightweight omnidirectional vision sensor," in *Proc. of IEEE Int. Conf. on Robotics and Automation (ICRA)*, 2014.

[19] S. Huh, D. Shim, and J. Kim, "Integrated navigation system using camera and gimbaled laser scanner for indoor and outdoor autonomous flight of UAVs," in *Intelligent Robots and Systems (IROS), IEEE/RSJ International Conference on*, 2013, pp. 3158–3163.

[20] B. Jutzi, M. Weinmann, and J. Meidow, "Weighted data fusion for UAV-borne 3D mapping with camera and line laser scanner," *International Journal of Image and Data Fusion*, 2014.

[21] A. Chambers, S. Achar, S. Nuske, J. Rehder, B. Kitt, L. Chamberlain, J. Haines, S. Scherer, , and S. Singh, "Perception for a river mapping robot," in *Proc. of IEEE/RSJ Int. Conf. on Intelligent Robots and Systems (IROS)*, 2011.

[22] K. Ok, S. Ansari, B. Gallagher, W. Sica, F. Dellaert, and M. Stilman, "Path planning with uncertainty: Voronoi uncertainty fields," in *Proc. of IEEE Int. Conf. on Robotics and Automation (ICRA)*, 2013.

[23] W. Green and P. Oh, "Optic-flow-based collision avoidance," *Robotics Automation Magazine, IEEE*, vol. 15, no. 1, pp. 96–103, 2008.

[24] S. Hrabar, G. Sukhatme, P. Corke, K. Usher, and J. Roberts, "Combined optic-flow and stereo-based navigation of urban canyons for a uav," in *Proc. of IEEE/RSJ Int. Conf. on Intelligent Robots and Systems (IROS)*, 2005.

[25] B. MacAllister, J. Butzke, A. Kushleyev, H. Pandey, and M. Likhachev, "Path planning for non-circular micro aerial vehicles in constrained environments," in *Proc. of IEEE Int. Conf. on Robotics and Automation (ICRA)*, 2013.

[26] H. Cover, S. Choudhury, S. Scherer, and S. Singh, "Sparse tangential network (SPARTAN): Motion planning for micro aerial vehicles," in *Proc. of IEEE Int. Conf. on Robotics and Automation (ICRA)*, 2013.

[27] C. Goerzen, Z. Kong, and B. Mettler, "A survey of motion planning algorithms from the perspective of autonomous uav guidance," *Journal of Intelligent and Robotic Systems*, vol. 57, no. 1-4, pp. 65–100, 2010.

[28] M. Quigley, K. Conley, B. P. Gerkey, J. Faust, T. Foote, J. Leibs, R. Wheeler, and A. Y. Ng, "Ros: an open-source robot operating system," in *ICRA Workshop on Open Source Software*, 2009.

[29] L. Meier, P. Tanskanen, L. Heng, G. Lee, F. Fraundorfer, and M. Pollefeys, "PIXHAWK: A micro aerial vehicle design for autonomous flight using onboard computer vision," *Autonomous Robots*, vol. 33, no. 1-2, pp. 21–39, 2012.

[30] D. Honegger, L. Meier, P. Tanskanen, and M. Pollefeys, "An open source and open hardware embedded metric optical flow cmos camera for indoor and outdoor applications," in *Proc. of IEEE Int. Conf. on Robotics and Automation (ICRA)*, 2013.

[31] D. Droeschel, M. Schreiber, and S. Behnke, "Omnidirectional perception for lightweight uavs using a continuous rotating laser scanner," in *Int. Arch. Photogramm. Remote Sens. Spatial Inf. Sci. (ISPRS)*, vol. XL-1/W2, 2013, pp. 107–112.

[32] J. Schneider, T. Läbe, and W. Förstner, "Incremental real-time bundle adjustment for multi-camera systems with points at infinity," in *ISPRS Archives of Photogrammetry, Remote Sensing and Spatial Information Sciences*, vol. XL-1/W2, 2013. [Online]. Available: http://www.int-arch-photogramm-remote-sens-spatial-inf-sci.net/XL-1-W2/355/2013/isprsarchives-XL-1-W2-355-2013.pdf

[33] D. Droeschel, J. Stückler, and S. Behnke, "Local multi-resolution representation for 6D motion estimation and mapping with a continuously rotating 3D laser scanner," in *Proc. of IEEE Int. Conf. on Robotics and Automation (ICRA)*, 2014.

[34] A. Geiger, M. Roser, and R. Urtasun, "Efficient large-scale stereo matching," in *Asian Conference on Computer Vision (ACCV)*, 2010.

[35] A. Hornung, K. M. Wurm, M. Bennewitz, C. Stachniss, and W. Burgard, "OctoMap: An efficient probabilistic 3D mapping framework based on octrees," *Autonomous Robots*, 2013.

[36] D. Applegate, R. Bixby, V. Chvatal, and W. Cook, "Concorde TSP solver," 2006.

[37] S. Ge and Y. Cui, "Dynamic motion planning for mobile robots using potential field method," *Autonomous Robots*, vol. 13, no. 3, pp. 207–222, 2002.

[38] M. Nieuwenhuisen, D. Droeschel, J. Schneider, D. Holz, T. Läbe, and S. Behnke, "Multimodal obstacle detection and collision avoidance for micro aerial vehicles," in *Proc. of European Conference on Mobile Robots (ECMR)*, 2013.